DOI: 10.13009/EUCASS2023-329
Aerospace Europe Conference 2023 – 10TH EUCASS – 9TH CEAS

Numerical simulation of phase change induced by pressure variations in cryogenic tanks

M. Deferrez[a], M. Bibal[b], S. Tanguy[b],A. Urbano[a†]
[a]*ISAE SUPAERO, Université de Toulouse, Toulouse, France*
[b]*Institut de Mécanique des Fluides de Toulouse (IMFT), Université de Toulouse, CNRS, Toulouse, France*
maxence.deferrez@isae-supaero.fr · annafederica.urbano@isae-supaero.fr
marie.bibal@isae-supaero.fr · tanguy@imft.fr
[†]Corresponding author

Abstract

Cavitation at the wall in tanks, characterised by fast bubbles growth in a superheated liquid, can be a great concern for cryogenic fluids storage in upper stages or fuel depots. Indeed, one cooling strategy, adopted in particular for conditioning the propellant before ignition, consists in depressurising the tank by venting the propellant, in order to create vapour and reduce the liquid propellant temperature. The tank thermal control is in the end strongly affected by phenomena arising at the bubble scale, and in the contact line region, that need to be predicted. In order to study these phenomena, without making use of sub-grid models for the phase change mass flow rate thermal gradients at the interface need to be solved with a direct numerical simulation (DNS). Moreover, for the simulation of pool cavitation, a compressible two-phase flow solver, including phase change, is required. In the present work, an innovative numerical algorithm for the DNS of compressible two-phase flows with phase change is presented. The solver is based on a level set/ ghost fluid approach, solves the complete set of Navier-Stokes conservation equations making use of a semi-implicit projection scheme. Cubic equations of state are used for the description of both the liquid, the vapour and the saturation conditions at the interface. In this paper the solver is introduced with particular attention devoted to the phase change modelling. The solver is used to investigate the cavitation of a methane bubble at the wall in micro-gravity conditions in a closed tank. After comparison with experimental data, a preliminary parametric study is carried out in order to investigate the influence of different depressurisation levels and rates on the bubble growth.

1. Introduction

Deep space exploration is an attractive and challenging topic that receives great attention in the space community today. The project for the future Lunar Gataway[1], that should prepare the path for future Mars missions, is an example of the large activity which is carried out in this field. In this context, Cryogenic Fluid Management (CFM) represents one of the main issues. Indeed, any large space mission will need cryogenic propellant that have high specific impulse Isp.[31] However, the drawback of cryogenics is that they have to be kept at low temperature, and phase change must be avoided. More generally, cryogenic fluids are substances that are in a vapour state at standard conditions but are stored in a liquid state at extremely low temperatures. They are used in various technologies such as scientific equipment, energy storage systems and in space applications. The transport and handling of cryogenic fluids pose challenges due to their tendency to undergo phase change, either through inertial effects (such as cavitation) or thermal effects (specifically boiling).[34] Boiling and cavitation, are two essential phenomena associated with phase change.[7] Boiling occurs if a liquid is brought to a superheated temperature, that is a temperature higher than the saturation temperature at the considered pressure. In particular, nucleate boiling refers to the process in which small bubbles nucleated in specific sites over a superheated wall grow under isobaric conditions. Cavitation, on the other hand, refers to phase change induced by pressure variation: it can occur when the pressure drops in a liquid and becomes lower than the saturation pressure.[5] If the pressure drop is induced by a flow (like for instance in a convergent nozzle) the phenomena is referred as *hydrodynamic cavitation*.[11,12] On the other hand, if the depressurisation is induced in a quiescent environment, like for instance in a tank when decreasing the pressure, the phenomena is referred as *pool cavitation*. Nucleation of the bubbles can occur either in the liquid core, for instance at the location of impurities, or at the wall.

[1] https://www.nasa.gov/feature/questions-nasas-new-spaceship

DOI: 10.13009/EUCASS2023-329

Several technological problems can be identified in relation with CFM and deep space exploration. In this paper the interest is on two specific applications for which CFM is a major issue: thermal control management of tanks for propulsive systems and refueling in space. Cryogenic propellants are stored near saturation conditions in the tanks. Therefore, during long duration phases, small temperature increases (a few K) could induce nucleate boiling. Consequences are an increase in the tank pressure and the presence of bubbles in the tank. On the other hand, the pressure in the tanks also need to be controlled in order to avoid cavitation in the pumps. During long duration coasting phases (for instance to reach Mars, or to insert multiple satellites in orbit) a thermodynamic equilibrium between the phases, at saturation conditions, will eventually be reached in a tank. Therefore, there is a necessity to cool down the propellant, in order to move away from the saturation conditions before restarting the engine. When cooling down the propellant, the pressure drops and cavitation could occur. The possible advantage of a in space propellant depot (ISCPD) is not a new concept. However, in the present space context it becomes a necessity in order to imagine possible future long-range exploration missions. Moreover, ISCPD could easier reusable vehicles development. Refueling in space could also be advantageous for other in-orbit services. Critical technology issues, related with CFM in micro-gravity, need to be addressed before these concepts can gain acceptance[6,8] and it has to be considered that all type of phase changes will occur when refueling: boiling, cavitation, film boiling. The receiver tank pressure and temperature will have to be controlled. Moreover, once the tank is full, a chill down procedure will have to be done before the engine can be started.

In both aforementioned applications, there is a need to control the temperature and pressure in tanks. Passive cooling, through Multi Layer Insulation (MLI), is not sufficient, and active cooling techniques are needed. This can be done with venting and non-venting systems. The main drawback associated with venting systems is the propellant loss. This is even more stringent in micro-gravity, because of the unknown position of the interface: liquid propellant could be loss. Moreover this will induce some forces on the system, and the dynamics will require a specific control. To suitably develop temperature and pressure control systems, there is clearly a need to understand the physics behind boiling and cavitation in micro-gravity. This will eventually allow a proper design of the whole system. This process start with the understanding of the basics phenomena at the bubble size level. In particular, among the aforementioned phase change phenomena, cavitation in micro-gravity is a challenging problem that we propose to address in this paper. Moreover, cavitation can be of interest also for other space applications, for instance in liquid rocket engines turbo-pumps. Even though, from a macroscopic point of view the cavitation in pumps differs from pool cavitation in tanks, at the bubble scale commonalities can be found.[12]

Cavitation occurring in a tank can be assimilated to acoustic cavitation. In fact, the phase change is induced by a pressure drop. The problem is complicated by the nature of cryogenic propellants, that are thermo sensible.[35] The bubble absorbs heat during cavitation, and this leads to a decrease of the temperature near the liquid phase interface. As a consequence, cavitation of cryogenic fluids cannot be assimilated with an isothermal process and thermal effects have to be taken into account. From a modelling point of view, this implies to consider the full set of governing equations to properly describe the phenomenon. Numerically, several approaches exist and are employed to simulate single bubble cavitation. More generally, the interaction between acoustics waves and interfaces is a problem that concerns a large number of different applications, from engineer to bio medical. Examples include atomisation in combustion chambers, sub-marines explosions and shock/bubble interactions and cavitation problems that are our main focus. To properly simulate these problems, a two phase compressible solver is needed. The numerical simulation of two-phase compressible flows is one of the main challenges for computational fluid dynamics. In fact, usually incompressible solvers are used to simulation two phase flows.[1,15,29,47] Those approaches cannot capture acoustics waves propagation. Complex numerical problems are associated with the numerical simulation of multi-phase compressibles flows. From one side this is caused by the great variation of the speeds of sound (from liquid to vapour) and to the corresponding small Mach numbers in the liquid phase. Another difficulty is associated with the proper thermodynamic description of both phases and of the saturation conditions at the interface. Different methodologies for the simulation of compressible two phase flows have been proposed during the last twenty years (see for instance[20] for a review). Most of these algorithms are based on "shock capturing" methodologies, using Riemann solvers. In particular a class of methods based on a semi-implicit projection approach have been developed for single phase and two phase flows.[23,48] The interest is that, while avoiding the acoustic time step constraint, these algorithms are asymptotically preserving.[20] However, most of these works are limited to non-viscous flows, and do not include non isentropic effects. The pressure projection methods have been extended to two-phase isentropic flows[13,17] and to two phase flows including viscous terms and heat conduction.[2,20,22] More recently phase change models have been considered in Duret et al.[9] and Martinez et al.[27] Most of these solvers are based on a conservative variables formulation, and non isentropic effects are considered in the total energy equation. However, while conserving the total energy, these approaches fail in retrieving a pressure consistent with the EoS at each iteration.[23] The solver used in the present paper is based on a semi-implicit projection scheme coupled with a level set/ghost fluid method to handle the interface and has been developed for the study of two-phase flows with phase change,[28,43] and has been integrated in the $\mathcal{DIVA}$ code[24,32,36,39–41] yet developed

DOI: 10.13009/EUCASS2023-329

for incompressible and variable density flows. It makes use of a generalised cubic Equation of State (EoS) to describe the vapour phase, the liquid phase and saturation conditions at the interface in a consistent way. Immersed Boundary Conditions allow the description of complex geometries. The major differentiating point of the present solver is that it uses a description of the conservation equations in terms of primitive variables with the energy conservation equation expressed in terms of pressure. The resulting Screened Poisson equation for the pressure accounts for non-isentropic terms. Moreover, a strong differentiating point of the present solver is the consistent thermodynamic description it ensures. In fact, it uses the same cubic EoS to describe the liquid the vapour and the saturation conditions at the interface. The algorithm allows to describe compressible two-phase flows problems driven by heat conduction, acoustic interface interaction and phase change phenomena induced by pressure and temperature variations. The objective of the present paper is to demonstrate the ability of the code in simulating phase change phenomena induced by temperature and pressure variations. In particular, attention will be given to bubble growth at the wall, including the presence of a contact line and of the conjugate heat transfer with the solid wall. The primary focus is to validate the accuracy and reliability of the present compressible solver through a comprehensive comparison with experimental data. Particular attention will be given to pool cavitation in micro-gravity conditions and on the driving parameters for the bubble growth. In the following first a brief overview of the solver is provided. Boiling configuration in isobaric environments are then investigated. For these configurations it is expected that the results are equal to what can be obtained with an incompressible solver and they aim at verifying the asymptotically preserving characteristics of the solver. Pool cavitation cases are then considered. Numerical results are first compared with experimental data. Finally, a preliminary investigation of the influence of pressure level and on the depressurisation speed on on pool cavitation phenomena is carried out in order to gain a deeper understanding of their interplay in microgravity environments.

2. Mathematical formalism for the description of compressible flows with phase change

2.1 Governing equations

The following form of the conservation equations for mass, momentum and energy in each phase, written in terms of primitive variables, i.e. the density ρ, the velocity vector $\vec{u}$ and the pressure p, are considered:

$$\frac{\partial \rho}{\partial t} + \nabla \cdot (\rho \vec{u}) = 0, \tag{1}$$

$$\frac{\partial \vec{u}}{\partial t} + \vec{u} \cdot \nabla \vec{u} + \frac{\nabla p}{\rho} = \frac{1}{\rho} \nabla \cdot \boldsymbol{\tau} + \rho \vec{g}, \tag{2}$$

$$\frac{\partial p}{\partial t} + \vec{u} \cdot \nabla p + \rho c^2 \nabla \cdot \vec{u} = \frac{c^2 \alpha}{c_p} \left[\boldsymbol{\tau} \otimes \nabla \vec{u} - \nabla \cdot \vec{q} \right]. \tag{3}$$

τ is tensor of viscous constraints, c is the local speed of sound, α is the local isobaric expansion coefficient , $\vec{g}$ is the gravity acceleration vector, c_p is the specific heat at constant pressure, $\vec{q} = -k \nabla T$ is local heat flux and T is the temperature where τ is defined as:

$$\tau = \mu \left(\nabla \vec{u} + \nabla \vec{u}^T \right) - \frac{2}{3} \mu \nabla . \vec{u} \mathbf{I} \tag{4}$$

and μ is the dynamic viscosity and $\mathbf{I}$ is the identity matrix. The following set of jump conditions at the interface Γ, that account for phase change, must be verified in order to maintain the conservation of mass, momentum and energy across the interface:[37]

$$[\vec{u}]_\Gamma = \dot{m} \left[\frac{1}{\rho} \right]_\Gamma \vec{n}, \tag{5}$$

$$[p]_\Gamma = \sigma \kappa + 2 \left[\mu \frac{\partial u_n}{\partial n} \right]_\Gamma - \frac{2}{3} \left[\mu \nabla \cdot \vec{u} \right]_\Gamma - \dot{m}^2 \left[\frac{1}{\rho} \right]_\Gamma, \tag{6}$$

$$[-k \nabla T \cdot \vec{n}]_\Gamma = \dot{m} h_{lv}, \tag{7}$$

where σ is the surface tension, h_{lv} is the latent heat of vaporisation, κ denotes the local interface curvature and u_n is the velocity component in the $\vec{n}$ direction, with $\vec{n}$ normal vector pointing towards the liquid phase.[14] The operator $[.]_\Gamma$ indicates the jump across the interface Γ . It is defined as $[f]_\Gamma = f_v - f_l$ with the subscripts l and v referring respectively to the liquid and vapour phases. The energy jump condition, Eq.(7), assumes that the interface is at the local saturation temperature ($T_\Gamma = T_{sat}$). Furthermore, thermodynamic equilibrium and zero entropy production at the interface are assumed, implying that the temperature is continuous across the interface ($[T]_\Gamma = 0$).[19]

DOI: 10.13009/EUCASS2023-329

2.2 Equation of state

An EoS is required to close the system of Eqs.(1)-(5). In the present work we will consider cubic EoS because they allow to describe liquid and vapour phases as well as the saturation conditions at the interface.[43] Among cubic EoS, the simulations in the present work are carried out considering the Patel-Teja-Valderrama (PTV)[46] EoS . The PTV EoS is expressed as:

$$p = \frac{\rho RT}{1-\rho b} - \frac{a\rho^2}{(1+b_1\rho)(1+b_2\rho)} \tag{8}$$

where $R = \mathcal{R}/\mathcal{M}$ is the gas constant, with $\mathcal{R} = 8314.46$ J/kmol/K universal gas constant and $\mathcal{M}$ molecular weight. The coefficients a, b , b_1 and b_2 are functions of the critical parameters and can be found in[46] and.[28]

2.3 Saturation conditions

Thermodynamic equilibrium is considered at the interface which is assumed to be at the saturation temperature T_{sat} at the pressure p_v in the vapour phase. There is a need to be able to evaluate saturation conditions at a specified pressure in order to impose the suitable condition at the interface. In this section the formalism that allows to deduce the saturation temperature T_{sat}, the saturation densities ρ_l ρ_g and the latent heat of vaporisation h_{hl} as a function of the pressure from a generalised cubic EoS summarised. The schematic representation in Fig.1 of an isothermal process based on a generalised cubic EoS in the (p, v) thermodynamic plan is used in order to illustrate these concepts. The specific volume $v = 1/\rho$ is used in this part instead of $1/\rho$.

Mechanical and thermodynamical equilibrium at the interface imply the following equality, known as Maxwell principle for phase equilibrium, is obtained[25] :

$$p_{sat}(v_g - v_l) = \int_l^v p dv\,, \tag{9}$$

The integral of the right hand side of Eq.(9) can be expressed analytically :

$$\int_l^v p dv = RT_{sat}\ln\left(\frac{v_g - b}{v_l - b}\right) - \frac{a}{(b_2 - b_1)}\ln\left[\frac{(v_g + b_1)(v_l + b_2)}{(v_l + b_1)(v_g + b_2)}\right], \tag{10}$$

where $\rho_g = \frac{1}{v_g}$ and $\rho_l = \frac{1}{v_l}$ are the two roots of Eq.(8) for $p = p_{sat}$ and $T = T_{sat}$. The saturation conditions (p_{sat}, T_{sat}) constitute the phase coexistence curve in the (p, T) plane, which has a slope provided by the Clausius Clapeyron equation:

$$\left.\frac{dp}{dT}\right|_{sat} = \frac{\Delta s}{\Delta v} = \frac{h_{lv}}{T_{sat}(v_g - v_l)}\,, \tag{11}$$

where $\Delta v = v_g - v_l = \frac{1}{\rho_g} - \frac{1}{\rho_l}$ is the specific volume change and $\Delta s = h_{lv}/T_{sat}$ the specific entropy change of the phase transition which can be expressed with the EoS considering an isothermal process at $T = T_{sat}$:

$$\Delta s = R\ln\left(\frac{v_g - b}{v_l - b}\right) - \frac{a'}{(b_2 - b_1)}\ln\left[\frac{(v_g + b_1)(v_l + b_2)}{(v_l + b_1)(v_g + b_2)}\right]. \tag{12}$$

DOI: 10.13009/EUCASS2023-329

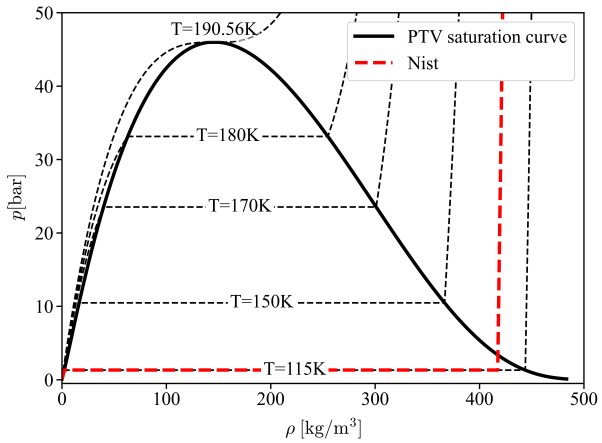

Figure 1: Pressure-Density diagram at saturation for the PTV EoS.

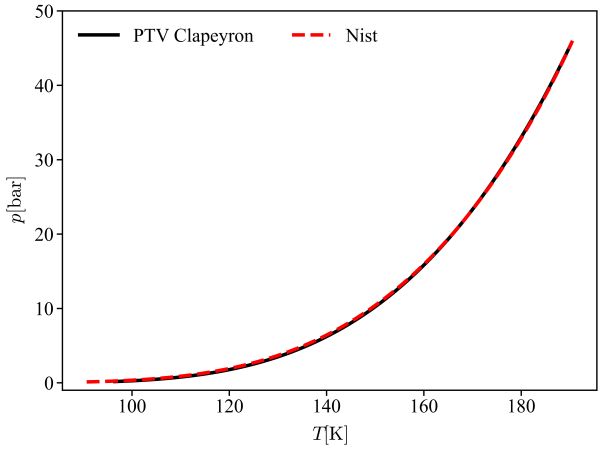

Figure 2: Pressure-Temperature diagram at saturation for the PTV EoS compared to Nist.

3. Numerical solver

Developing a numerical solver for two-phase compressible flows with phase change is a challenging objective because of several reasons. First, the numerical method able should be able to account for acoustic propagation in low-Mach number flows. Second the solver should be able to simulate capillary based phenomena. Last but not least, the solver should be able to simulate phase change phenomena. This last requirement implies to have an accurate estimation of the thermal gradients at the interface and a thermodynamic formulation able to describe liquid, vapour and saturation conditions in a consistent way. All the above requirements must be met while ensuring numerical stability and convergence capabilities of the solver. In the present section, some details on an innovative numerical method for the simulation of phase change phenomena in compressible flows of single species are presented, and more details can be found in[28] The following split is operated to the primitive variables:

$$\rho = \rho_0 + \rho_{st}\,, \qquad \vec{u} = \vec{u}_0 + \vec{u}_{st}\,, \qquad p = p_0 + p_{st}\,, \tag{13}$$

where u_{st} is the solenoidal part of the velocity field, we have $\nabla.\vec{u}_{st} = 0$ and $\rho_{st} = const$. For simplicity we will set $\rho_{st} = 0$. Once the splitting is integrated in the system of Eqs.(1)-(3), and the temporal discretisation is carried out the following Screened poisson equation for p_0 is obtained:

$$\frac{(p_0)^{n+1}}{(\rho c^2)^n} - \Delta t^2 \nabla \cdot \left(\frac{\nabla p_0}{\rho}\right)^{n+1} - \Delta t \left(\frac{\alpha}{\rho c_p}\right)^n \nabla \cdot (k \nabla T^{n+1}) = \frac{p^* - p_{st}^{n+1}}{(\rho c^2)^n} - \Delta t \nabla \cdot \vec{u}_0^* + \Delta t \left(\frac{\alpha}{\rho c_p}\right)^n \left[\boldsymbol{\tau}^n \otimes \nabla \vec{u}^n\right]. \tag{14}$$

where $p^* = p^n - \Delta t(\vec{u}^n \cdot \nabla p^n)$. A level set approach is used to track the interface with a Ghost Fluid method to handle the sharp jump accros the interface.[10,38] Therefore, ghost fields for ρ and p_{st} are defined, with constant extrapolations.[3] The solver is implemented in the $\mathcal{DIVA}$ code that has been extensively validated for the simulation of two phase incompressible flows with and without phase change ([24,32,36,39–41,44,45]). The methodology developed for phase change for incompressible flows is adapted to the compressible flow solver in.[?] Therefore, ghost fields will be defined for the velocities and temperature fields. Phase change mass flow rate will be computed according to Eq.(7), and the corresponding jump in the velocity field (Eq.(5)) will be imposed on the ghost velocity fields. The Dirichlet boundary condition imposed at the interface, $T_\Gamma = T_{sat}$, will be deduced from the liquid vapour equilibrium condition and the local pressure. The phase change mass flow rate $\dot{m}$ is evaluated using the energy jump condition Eq.(7) once the temperature gradients at the interface are known:[36,42]

$$\dot{m} = \frac{-k_v \nabla T_v \cdot \vec{n} + k_l \nabla T_l \cdot \vec{n}}{h_{lv}}\,, \tag{15}$$

where the h_{lv} is evaluated from the EoS as explained in section 2.3. The $\dot{m}$ is calculated on a few cells around the interface and an extrapolation of the mass flow rate is performed in order to extend continuously the mass flow rate

DOI: 10.13009/EUCASS2023-329

in the computational field from the interface location. The Clausius Clapyeron equation is used to update saturation conditions at each time step in a few cells around the interface according to:

$$T_{sat}^{n+1} = T_{sat}^{n} + \frac{p_{sat}^{n+1} - p_{sat}^{n}}{\Delta s^{n}} \left(\frac{1}{\rho_{v,sat}^{n}} - \frac{1}{\rho_{l,sat}^{n}} \right), \tag{16}$$

$\rho_{v,sat}^{n+1}$ and $\rho_{l,sat}^{n+1}$ are computed solving Eq.(8) for p_{sat}^{n+1} and T_{sat}^{n+1} using the Cardan's method.[43]

The time step Δt is limited by classical stability conditions on convection, viscosity, surface tension and conduction :

$$\frac{1}{\Delta t} = \frac{1}{\Delta t_u} + \frac{1}{\Delta t_\mu} + \frac{1}{\Delta t_\sigma} + \frac{1}{\Delta t_k}. \tag{17}$$

Δt_μ, Δt_u, Δt_σ and Δt_k are given by :

$$\begin{aligned}
\Delta t_u &= CFL_u \frac{\Delta x}{max||\vec{u}||} \\
\Delta t_\mu &= CFL_\mu \frac{1}{2} \frac{max(\rho)\Delta x^2}{max(\mu)} \\
\Delta t_\sigma &= CFL_\sigma \frac{1}{2} \sqrt{\frac{min(\rho)\Delta x^3}{\sigma}} \\
\Delta t_k &= CFL_k \frac{\theta_{lim}}{4} \frac{min(\rho)\Delta x^2}{max(k)},
\end{aligned} \tag{18}$$

Δx is an indicator of the size of the smallest cell in the domain. CFL_u, CFL_μ and CFL_σ are smaller or equal to 1 and CFL_k can be higher than 1 if the thermal conduction term is treated with an implicit scheme. $\theta_{lim} = 0.1$ for all the simulations presented in this paper. More details are provided in.[28]

4. Nucleate Boiling

Nucleate boiling is a complex heat transfer phenomenon that occurs in various engineering and industrial applications. It is characterised by the formation of vapour bubbles on heated surfaces, followed by their growth and detachment when under gravity influence. Previous studies have explored the numerical simulation of nucleate boiling using the $\mathcal{DIVA}$ incompressible solver. Notably, Huber and al[18] conducted a study, demonstrating its capability to accurately capture the phase change phenomena and growth rates of bubbles in normal gravity conditions. Building upon this foundation, the present study focuses on employing the developed compressible solver to verify its ability to simulate nucleate boiling which is an isobaric phenomena for which incompressible assumption can be done. The computation domain is a cylinder of height $H = 8$ mm and radius $R = 4$ mm and it is shown in Fig.(3) where the boundary conditions are described. Axisymmetric simulations are carried out, using a cartesian grid. The upper wall is open, the lateral wall is adiabatic and the bottom wall is kept at a constant temperature T_w. The liquid is initially at saturation conditions ($p_{sat} = p_{sat}(T_{sat})$) everywhere but in a boundary layer near the wall where the temperature varies from T_{sat} towards T_w, leading to a thermal boundary layer where the bubble is immersed. The thickness δ of the thermal boundary layer which is computed from the correlation of Kays and Crawford[21] for free convection given by Eq.(19):

$$\delta = 7.14 \left(\frac{\mu_l \alpha_l}{\rho_l g \beta_l \Delta T} \right)^{1/3}. \tag{19}$$

The temperature difference $\Delta T = T_w - T_{\text{sat}}$, referred to as the superheat, leads to the definition of the non dimensional Jakob number (Ja):

$$\text{Ja} = \frac{c_{p_l}}{h_{lv}} \frac{\rho_l}{\rho_v} \Delta T. \tag{20}$$

The thermodynamic properties used in the simulation are defined in Table.(1), with $\Delta T = 23.7$K, leading to Ja = 25. An arbitrary apparent angle θ_{app} of 50°is used for the simulations. The contact angle is imposed as a boundary condition on the level set function at the bottom wall. The radius of the initial vaopour seed is $R_i = 200\ \mu$m.

The same simulation is carried out with the compressible and incompressible solvers. Specifically, the thermodynamic properties computed with the models of the compressible solver are used for the incompressible simulations in which they are kept constant ($c_{p,l}$, $c_{p,v}$, ρ_v and ρ_l). In particular, considering that there is a stratification of the temperature both in the liquid and in the vapour those thermophysical properties vary in space and time in the compressible simulations. Average values are considered in the incompressible simulations. However, a strict and exact comparison

DOI: 10.13009/EUCASS2023-329

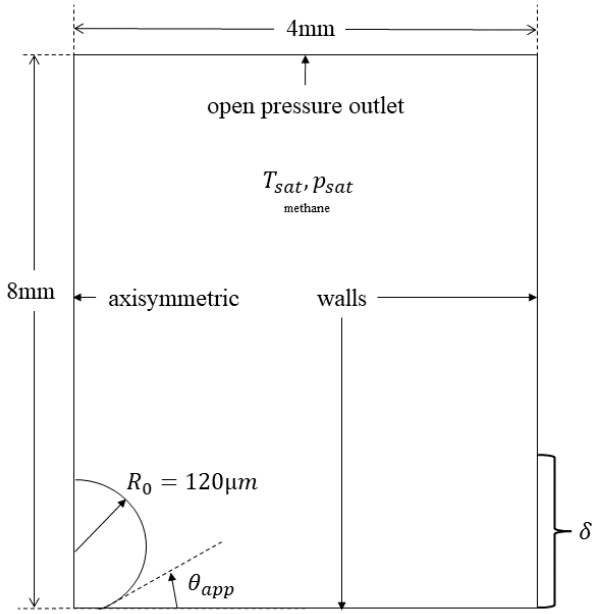

Figure 3: Boundary conditions of the nucleate boiling simulation.

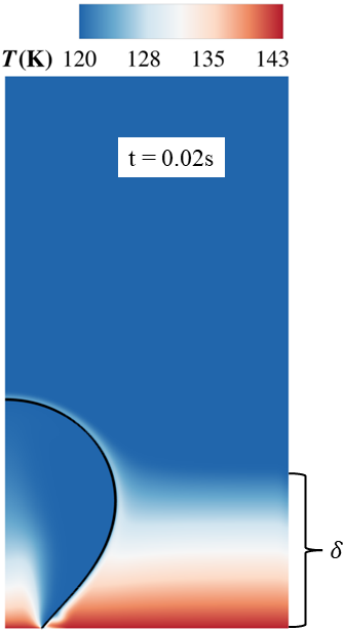

Figure 4: Instantaneous 2D field of the temperature at t=0.02s.

Table 1: Thermophysical properties for methane for the vapour at p_{sat} = 1.768 bar and T_{sat} = 120 K.

	ρ	μ	k	c_p	σ	h_{lv}
	[kg/m^3]	[Pa.s]	[W/K/m]	[J/kg/K]	[N/m]	[J/kg]
liquid	434.66	0.988×10^{-6}	0.17792	3203.07	0.013	0.5172×10^{6}
vapour	3.226	4.63×10^{-6}	0.011995	1590.10	-	-

will therefore not be possible. The same simulation is carried out with a mesh refinement of 16, 8 and 4 μm. An example of an instantaneous 2D temperature field obtained with the compressible solver at t=0.2 s is shown in Fig.(4). The temporal evolution of the equivalent radius evolution obtained with the two solvers and the differents meshes are shown in Fig.(5). It is observed that as the mesh is refined, the compressible solver solution tends toward the incompressible one. However, the compressible solver does not show a numerical convergence, whereas the incompressible does. A further simulation, with a mesh size of 2μm is necessary to conclude and will be the scope of a future work. The comparison can be done also in terms of detachment diameters which are illustrated in Fig.(6). It is observed that the compressible solver yields slightly lower detachment diameters compared to the incompressible solver for each mesh refinement. However, as the difference between two consecutive mesh refinements becomes smaller, the detachment diameters converges, and the two solvers results get closer.

5. Pool cavitation

Pool cavitation refers to the formation and behaviour of a bubble under varying pressure conditions, and the present work focuses on single bubble cavitation attached to a solid wall, that is in presence of a contact line. In a liquid/vapour phase system in equilibrium saturation conditions, if the pressure is decreased, the liquid will become superheated, thus favouring the growth of bubbles in a superheated liquid. In particular in the present paper we are interested in bubble cavitating in a zero-gravity environment. Axisymmetric simulations of single bubbles will be carried out. The computational domain is a cylinder, initially filled with liquid methane in saturation conditions. All the walls are adiabatic. The pressure is decreased in time thus inducing a decrease of the saturation temperature at the interface: as a consequence the liquid become superheated and the bubble grows. The aim of the present work is first to validate the ability of the solver in simulating phase change induced by pressure variations. The second objective is to investigate the phenomena driving the bubble growth. Finally, the aim is to carry out a parametric study in order to investigate the impact of the depressurisation over the bubble behaviour.

DOI: 10.13009/EUCASS2023-329

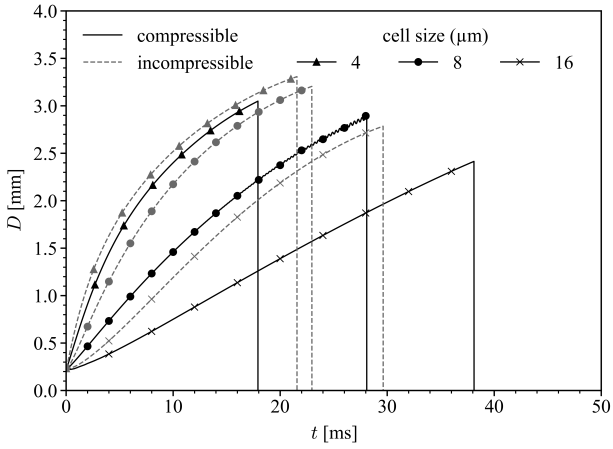

Figure 5: Comparison of the bubble diameter evolution in time computed with the compressible and incompressible solvers for different mesh refinements.
$R_0 = 120\ \mu$m; $\theta_{app} = 50°$; $p_{sat} = 1.768$ bar; $T_{sat} = 120$ K.

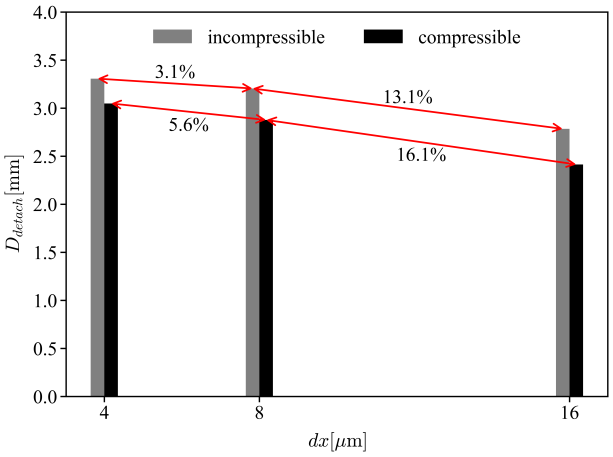

Figure 6: Comparison of the compressible and incompressible detachment bubble diameters for different mesh refinements.

5.1 Experimental comparison

To assess the capability of the solver in simulating phase change induced by pressure variation in the presence of a contact line, an experimental reference case is considered. Experimental data obtained from a recent experiment conducted in the drop tower of ZARM (Center of Applied Space Technology and Microgravity) by Niklas Weber and Michael Dreyer has been made available to the researchers through private communications. The experiments features the growth of a single methane bubble induced by a depressurisation in micro-gravity conditions. The experimental data provided includes measurements of the bubble's growth over time in terms of its radius, as well as the corresponding pressure imposed in the chamber during the microgravity time frame in Fig.(9). The pressure profile is used as a boundary condition for the numerical simulation. The growth of the bubble over time, as captured in the experimental data, serves as a valuable benchmark for evaluating the accuracy of the numerical model. By comparing the simulated bubble growth obtained from the compressible solver with the experimental measurements, insights can be gained into the solver's ability to capture the dynamics and behavior of the pool cavitation bubble under varying pressure conditions. This comparison between the compressible solver and the experimental data from Zarm's drop tower experiment not only serves to validate the numerical model but also provides an opportunity to further understand pool cavitation phenomena. The agreement or discrepancies between the simulated and experimental results can shed light on the underlying physics and mechanisms involved in pool cavitation, and potentially highlight areas for future research and model refinement.

The boundary conditions for simulating pool cavitation are described in Fig.(7). The simulation domain consists of a solid wall in contact with a surrounding fluid with an initial bubble's germ of radius R_0 of 40μm. The domain is a cylinder of height 6 mm and radius 6 mm. The solid wall has thickness of 0.375 mm. Heat conduction in the wall is accounted for with a proper solver for the energy equation in the solid domain,[44] which has been coupled with the compressible solver. An axisymmetric simulation is carried out with a uniform grid of 1024×1024 points corresponding to cell size of $\Delta x = 6\ \mu$m. Boundary conditions at the solid/fluid interface impose the temperature continuity and the equality of the heat fluxes. A pressure variation is imposed in the upper wall with the profile reported in Fig. 9 corresponding to the experimental data. To initialise the simulation, both the fluid and solid fields are set to saturation conditions corresponding to the PTV EoS: $p_0 = 1.44$ bar; $T_0 = T_{sat}(p_0) = 117.28$ K. The thermodynamic properties of the fluid used in the simulation are summarised in Table2. The thermodynamic properties of the wall are summarised in Table 3 and the apparent contact angle is $\theta_{app} = 5°$. Indeed methane is considered to be a wettable fluid. The microscopic contact angle is expected to be very small, around 0. However, in the present simulations the resolution is higher the micro-region dimension which extends in the first 100 nm, and where the contact angle is expected to vary from a microscopic towards an apparent contact angle, which can be imposed as a boundary condition in the present simulations. A preliminary parametric study (not shown here) was done varying the apparent contact angle from 15 to 0. The study demonstrated that there is no influence on the bubble's growth from the θ_{app} under 10°, even for a θ_{app} of 0°.

DOI: 10.13009/EUCASS2023-329

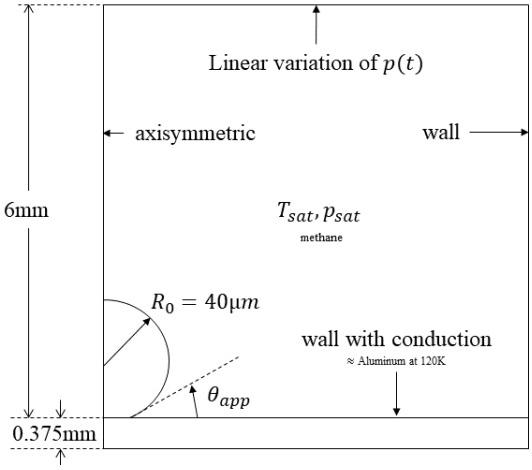

Figure 7: Computational domain and boundary conditions for the pool cavitation test case. Thermodynamical properties for the solid wall material: alluminium : ρ_w = 2700 $kg.m^{-3}$, c_{p_w} = 8970 $J.kg^{-1}.K^{-1}$, k_w = 240 $W.m^{-1}.K^{-1}$.

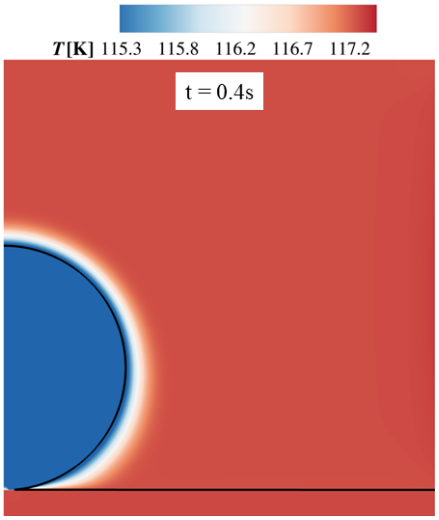

Figure 8: Instantaneous 2D field of the temperature at t=0.4s.

Table 2: Thermophysical properties of methane for the gas at p_{sat} = 1.404 bar and T_{sat} = 116.7 K.

	ρ [kg/m^3]	μ [Pa.s]	k [W/K/m]	c_p [J/kg/K]	σ [N/m]	h_{lv} [J/kg]
liquid	440.78	1.15×10^{-6}	0.17792	3144.05	0.012	0.52015×10^{6}
vapour	2.42	4.3×10^{-6}	0.011995	1592.64	-	-

Table 3: Thermophysical properties of the wall at T_{sat} = 116.7 K.

ρ_w [kg/m^3]	c_{p_w} [J/kg/K]	k_w [W/K/m]
2700	8970	240

DOI: 10.13009/EUCASS2023-329

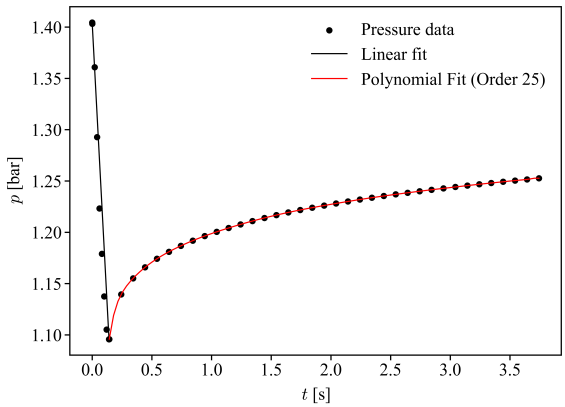

Figure 9: Pressure boundaries limits of the simulation for reproducing ZARM's experiment conditions (data from private communications with N. Weber and M. Dreyer.

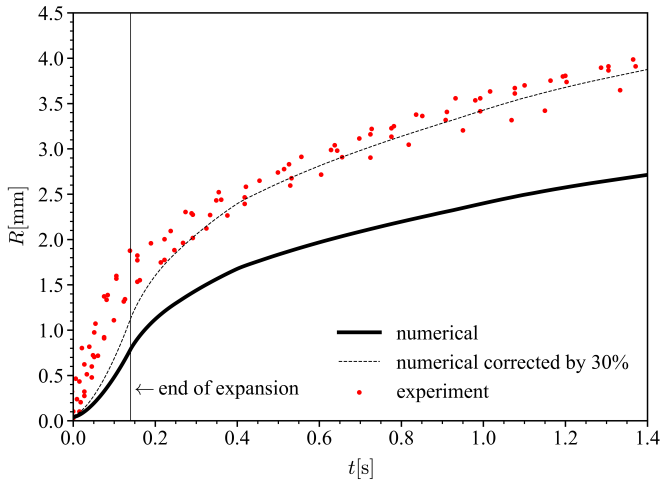

Figure 10: Comparison of the bubble radius evolution in time with Zarm's experiment. R_0 = 40 μm; θ_{app} = 5°; p_0 = 1.44 bar; T_0 = 117.28 K; $1 - \frac{p_f}{p_0}$ = 24.4 %; dx = 6 μm.

An example of an instantaneous 2D field of temperature at t = 0.4 s is shown in Fig.(8), when p=1.162 bar (see Fig. 9). The corresponding saturation temperature imposed at the interface at that instant is T = 114.77 K. It appears indeed how the temperature in the liquid and in the solid domain are close to the initial temperature T_0. On the other hand, the temperature in the bubble is lower and equal to $T = T_{sat}(p)$ = 115.4 K . The liquid is superheated and phase change between the liquid and the vapour phase is occurring. The evolution of the equivalent radius in time is compared in Fig.10 with experimental data. In the first part of the simulation, for t < 130 ms, the pressure is decreasing. Consequently the bubble growth is induced by two phenomena: the bubble expansion and the phase change mass flow rate. We will call this phase the *expansion phase*. For t > 130 ms the tank is closed and the bubble growth is induced by the phase change only. We will call this phase the *diffusive phase*. The two phases are clearly visible in both the experimental and numerical data, and are characterised by two different slopes of the diameter curve evolution. The simulation results exhibit a consistent and favorable slope, indicating a commendable agreement with experimental data. This agreement indicates that the compressible solver accurately models the fundamental dynamics of the pool cavitation process ans that the solver's underlying numerical algorithms effectively account for the pressure variations and fluid-solid interactions that drive bubble growth. However, from a quantitative point of view , the difference between the two diameters is of approximately 30% as reported in Fig. 10.

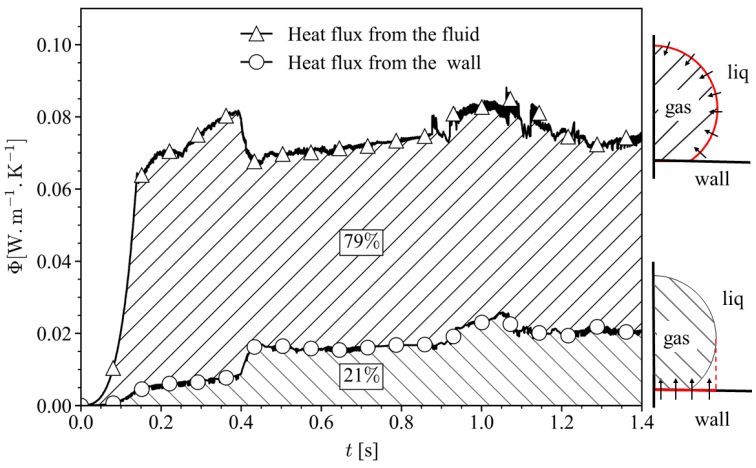

Figure 11: Temporal evolution of the heat flux going in the bubble from the superheated liquid (triangle) and from the wall (circle). Comparison of the heat flux source showing the contribution in percentage of each source integrated over time.

To gain insight into the factors contributing to the deviation between the numerical simulation and the experimen-

DOI: 10.13009/EUCASS2023-329

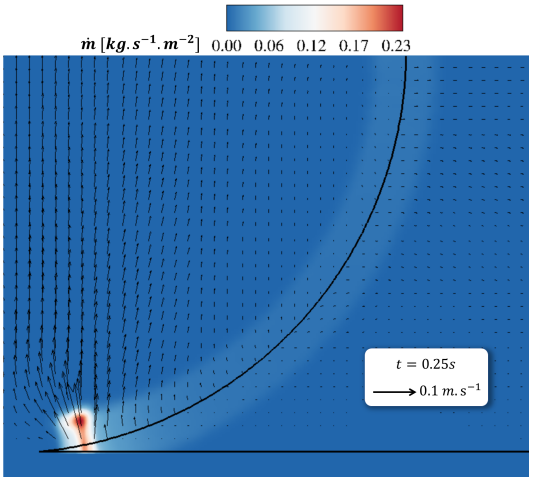

Figure 12: 2D field of the surface mass flow rate with velocity vectors.

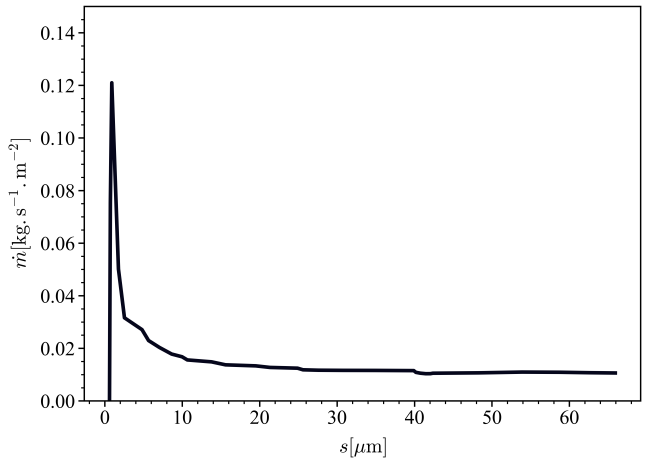

Figure 13: Distribution of the surface mass flow rate along s, the curvilinear abscissa,t = 0.1s.

tal data, a detailed analysis of heat transfer and mass flow rate distribution along the interface is conducted. Fig. (11) illustrates the heat transfer contributions from the wall and the surrounding liquid to the bubble. By examining the distribution of heat flux, it becomes possible to understand the relative impact of each heat transfer mechanism on the bubble growth. It appears that approximately 21% of the total heat flux going in the bubble originates from the wall, and 79% from the surrounding liquid. Therefore, even if the heat flux from the wall is of minor importance with respect to the one from the superheated liquid, it is not negligible. It is therefore expected that that the thermal interaction between the wall and the bubble significantly influences the growth rate observed in the numerical simulation. Furthermore, Fig. (12) presents the field of the surface mass flow rate at $t = 0.25$ s of the simulation. This visual representation allows to observe the spatial distribution of the mass flow rate along the interface. Analysing the mass flow rate distribution aids in understanding how the fluid is interacting with the bubble surface and influencing its growth behaviour. To complement the analysis, Fig. (13) provides the distribution of the surface mass flow rate along the interface, s being a curvilinear abscissa that originates at the contact line. This one-dimensional representation enables a more focused examination of the mass flow rate variation and its impact at specific locations along the bubble surface. One notable observation is that the specific phase change mass flow rate has a pick in the vicinity of the contact line, in a region having an extension of a few micrometers, as usually observed in nucleate boiling simulations. This is the consequence of the high temperature gradients established in this region between the wall at T_w and the interface at T_{sat}. Moreover, the phase change masse flow rate eventually reaches a null value at the contact line. In fact, at the contact line the wall is locally thermalised at $T_w = T_{sat}$ and therefore there is no heat flux at the contact line. However, in particular for highly wettable fluids, it is expected that a micro-region exists extending over distance of the order of 100 nm after the contact line. This micro-region, driven by the presence of a interface resistance at the contact line, induced a bending of the interface from the microscopic contact angle θ_{mic} towards the apparent contact angle θ_{app} outside the micro-region, and important associated heat fluxes. A micro-region model could be of primordial importance in the present case for two reasons. First, in order to impose the correct θ_{app} . Secondly, in order to include the micro-region heat flux and associated phase change mass flow rate that could modify the bubble growth. The substantial heat transfer contribution from the wall underscores the importance of accurately capturing the heat transfer mechanisms occurring at the solid-fluid interface and considering a micro-region model could strongly amplify the heat flux coming from the wall. This suggests that incorporating a micro-region model could be crucial for achieving a more precise prediction of the growth rate and improving the agreement with the experimental data. No micro-region model has been included so far and will be the scope of future works. In summary, this preliminary comparison between experimental data and numerical simulation for the pool cavitation of a single bubble allows to demonstrate that the solver is able to retrieve the fundamental mechanisms associated with the phenomena, that is expansion and phase change, as demonstrated by the correct reproduction of the slopes of the diameter evolution in time. Further investigations are required to analyse and hopefully reduce the discrepancy in terms of diameter. Various factors, including fluid properties, pressure conditions, and interfacial dynamics phenomena such as the micro-region, could contribute to these differences. Besides, a proper convergence analysis has not been carried out so far. These will be investigated in future works.

DOI: 10.13009/EUCASS2023-329

5.2 Parametric analysis for the characterisation of a bubble growth induced by cavitation

In the present section a parametric study carried out in order to characterise the bubble growth induced by cavitation in conditions similar to the one investigated in the experimental case of section 5.1. The computational domain and the initial conditions in the liquid methane are unchanged, but the pressure evolution at the bottom boundary, for $t < \Delta t$, is imposed with the following linear law:

$$p(t) = p_i + \frac{p_0 - p_f}{\Delta t} t\,, \tag{21}$$

where p_0 and p_f are the pressures at the beginning and end of the expansion phase that has a duration fo Δt s. After the expansion phase, for $t > \Delta t$ the pressure is kept constant and equal to $p = p_f$. Two parametric studies are carried out varying either the depressurisation level $\Delta p = p_0 - p_f$ and the depressurisation rate driven by Δt.

It is possible to define a Jakob number associates to the Δp as follow :

$$\mathrm{Ja} = \frac{\rho_l}{\rho_\mathrm{v}} \frac{c_{pl} T_{sat}}{h_{lv}^2} \left(\frac{1}{\rho_\mathrm{v}} - \frac{1}{\rho_\mathrm{l}} \right) \Delta p, \tag{22}$$

where the superheat ΔT has been expressed as a function of the depressurisation Δp making use of Clausius Calpeyron relation Eq.(11).

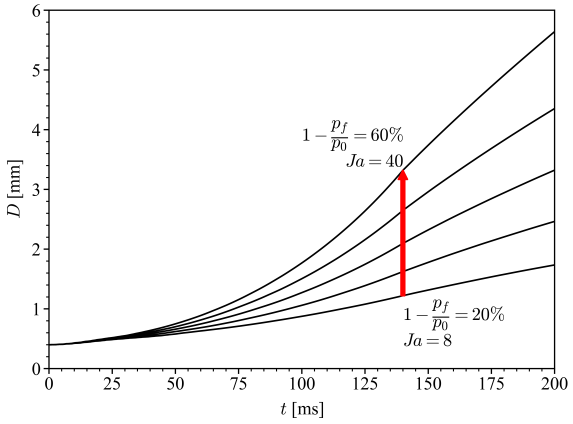

Figure 14: Comparison of the bubble diameter evolution in time with different pressure ratio for cavitating boiling simulation.
R_0 = 200 μm; θ_{app} = 5 °; p_0 = 1.44 bar; T_0 = 117.28 K; dx = 32 μm.

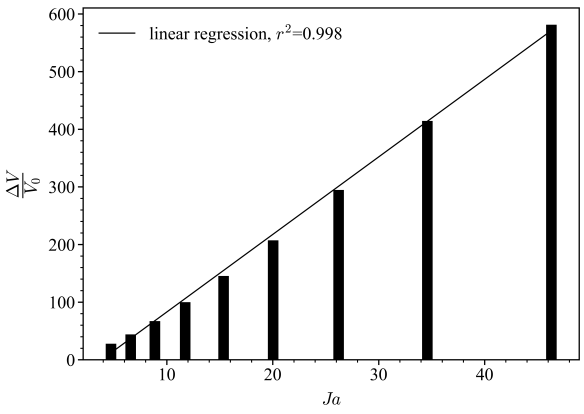

Figure 15: Bubble's vapour volume created for different Jakob number, for a fixed expansion duration Δt

DOI: 10.13009/EUCASS2023-329

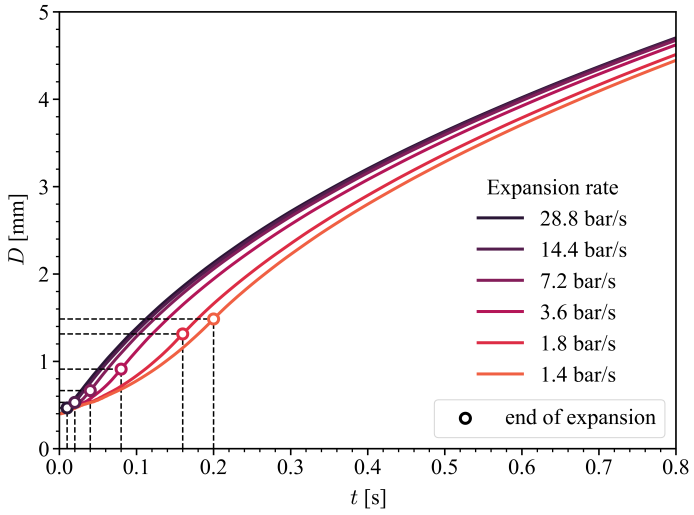

Figure 16: Comparison of the bubble diameter evolution in time with different expansion rate for cavitating boiling simulation.
R_0 = 200 μm; θ_{app} = 5 °; p_0 = 1.404 bar; T_0 = 116.7 K; $1 - \frac{p_f}{p_0}$ = 20 %; dx = 32 μm.

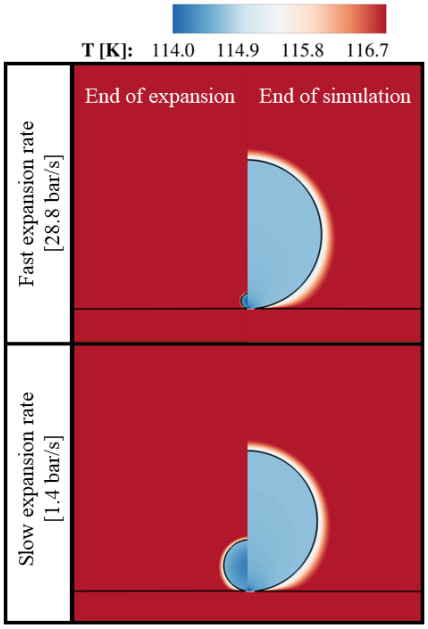

Figure 17: Temperature field obtained for a fast (top) and slow (bottom) expansion rates, at the end of the expansion phase (left) and at the end of the simulation in the diffusive phase (right). R_0 = 200 μm; θ_{app} = 5 °; p_0 = 1.404 bar; T_0 = 116.7 K; $1 - \frac{p_f}{p_0}$ = 20 %; dx = 32 μm.

Fig.(14) illustrates the temporal evolution of the bubble diameter obtained for different Ja, varying from Ja=8 up to J=40, corresponding to a Δp varying between 20 and 60 % of the initial pressure p_0. The red arrow indicates the end of the expansion phase. As expected, the diameter of the bubble and its growth rate increase with Ja. This observation aligns with the expected behaviour, as higher Ja indicate a greater availability of heat for bubble growth. Moreover, in Fig.(15) are shown vapour volume variations ΔV during the expansion phase as function of the Ja, revealing a linear evolution of ΔV with Ja. This suggests that the Ja number plays a crucial role in determining the amount of vapour generated at the end of the expansion, providing a valuable insight into the dynamics of cavitation and its dependence on the thermodynamic conditions. The results of the investigation of the influence of the expansion rates, obtained by varying the Δt for a same Δp = 20% corresponding to a Ja=8, are shown in Fig.(16) and Fig.(17). Faster expansion rates result in larger bubble diameters. However, it is noteworthy that even with significantly different expansion rates, the resulting bubble diameters at the end of the simulation are not substantially different. This observation suggests that the expansion rate, while influential, may have a slightly lesser impact on bubble size after the diffusive phase. Further analysis in Fig.(17) provides additional insights into the temperature field after the expansion ends for simulations with different expansion rates. Interestingly, despite significant differences in the temperature field during the final stages of the expansion, the temperature fields converge to a similar pattern after a few hundred milliseconds in the diffusive phase. These preliminary parametric studies ndicate that the long-term behavior of the system is less sensitive to the initial differences in expansion rates. These insights contribute to our understanding of the phenomena involved in pool cavitation and provide guidance for the development of accurate and efficient modelling approaches.

6. Conclusion

This study has provided valuable insights into the dynamics and characteristics of nucleate boiling and pool cavitation through a combination of numerical simulations, experimental comparisons, and parametric studies. The validation of the compressible solver against experimental data has demonstrated its capability to accurately capture the growth rate of nucleate boiling bubbles and the behavior of pool cavitation under microgravity conditions. Although some deviations were observed between the simulation and experimental results, the overall trends and important features were effectively captured. The analysis of heat transfer contributions from the wall and the liquid to the bubble has highlighted the significant influence of the wall on bubble growth, indicating the importance of accurately modeling the micro-scale phenomena near the contact line. The examination of mass flow rate distributions has revealed a profile

DOI: 10.13009/EUCASS2023-329

similar to the one typical of nucleate boiling, with a pick in the region near the contact line. These findings emphasise the need for incorporating a micro region model to fully converge and accurately capture phase change phenomena in presence of a contact line. Parametric studies investigating the effects of expansion rates and Jakob numbers have provided important insights into the growth of a bubble induced by pool cavitation. The results showed that the Ja number has a considerable impact on the growth rate, while the expansion rate exhibited a lesser influence. Overall, this study underscores the importance of accurately modelling the complex phenomena involved in nucleate boiling and pool cavitation. The validation of the compressible solver and the understanding gained through this research contribute to the development of enhanced models that incorporate micro-scale effects, Jakob numbers, and expansion rates. Such advancements are crucial for predicting and optimizing pool cavitation processes in various industrial applications, leading to improved system performance, safety, and efficiency.

7. Acknowledgments

The authors gratefully acknowledge Niklas Weber and Michael Dreyer for giving access to the data from their drop tower experiment, and for fruitful discussions on pool cavitation.

The authors gratefully acknowledge ESA-ESTEC for co-funding the PhD thesis of Maxence Deferrez, and S. Vincent Bonnieu for his advices and support.

This work was supported by the Chair for Advanced Space Concepts (SaCLab2) resulting from the partnership between Airbus Defence and Space, Ariane Group and ISAE-SUPAERO.

References

[1] G. Agbaglah, R. Chiodi, and O. Desjardins. Numerical simulation of the initial destabilization of an air-blasted liquid layer. *J. Fluid Mech.* , 812:1024–1038, 2017.

[2] M. Arienti and M. Sussman. A numerical study of the thermal transient in high-pressure diesel injection. *Int. J. Multiphase Flow* , 88:205–221, 2017.

[3] Tariq D. Aslam. A partial differential equation approach to multidimensional extrapolation. *J. Comput. Phys.* , 193(1):349–355, 2004.

[4] J. Bae, J. Yoo, L. Jin, and S. Jeong. Experimental investigation of passive thermodynamic vent system (tvs) with liquid nitrogen. *Cryogenic* , 89:147–156, 2018.

[5] C. E. Brennen. *Cavitation and bubble dynamics*. Oxford University Press, 1995.

[6] D. J. Chato. Cryogenic fluid transfer for exploration. *Cryogenic* , 48:206–209, 2008.

[7] C. Colin, O. Kannengieser, W.Bergez, M.Lebon, J.Sebilleau, and S.Tanguy M.Sagan. Nucleate pool boiling in microgravity: Recent progress and future prospects. *Comptes Rendus Mecanique* , 2017.

[8] C.H. DeLee, P. Barfknecht, S. Breon, R. Boyle, M. DiPirro, J. Francis, J. Huynh, X. Li, J. McGuire, S. Mustafi, J. Tuttle, and D. Wegel. Techniques for on-orbit cryogenic servicing. *Cryogenic* , 64:289–294, 2014.

[9] B. Duret, R. Canu, J. Reveillon, and F.X. Demoulin. A pressure based method for vaporizing compressible two-phase flows with interface capturing approach. *Int. J. Multiphase Flow* , 108:42–50, 2019.

[10] Ronald P Fedkiw, Tariq Aslam, Barry Merriman, and Stanley Osher. A non-oscillatory eulerian approach to interfaces in multimaterial flows (the ghost fluid method). *J. Comput. Phys.* , 152(2):457–492, 1999.

[11] A. Ferrari. Fluid dynamics of acoustic and hydrodynamic cavitation in hydraulic power systems. *Proc. R. Soc. Lond. A* , 473:20160345, 2017.

[12] J.-P. Franc and J.-P. Michel. *Fundamentals of Cavitation*. Kluwer Academic Publishers, 2004.

[13] D Fuster and S Popinet. An all-mach method for the simulation of bubble dynamics problems in the presence of surface tension. *J. Comput. Phys.* , 374:752–768, 2018.

[14] F. Gibou, L. Chen, D. Q. Nguyen, and S. Banerjee. A level set based sharp interface method for the multiphase incompressible navier-stokes equations with phase change. *J. Comput. Phys.* , 222:536–555, 2007.

[15] M. Gorokhovski and M. Herrmann. Modeling primary atomization. *Ann. Rev. Fluid Mech.* , 40:343–366, 2008.

DOI: 10.13009/EUCASS2023-329

[16] J. W. Hartwig. Propellant management devices for low-gravity fluid management: Past, present, and future applications. *J. Spacecrafts and Rockets* , 54(4):808 – 824, July - August 2017.

[17] G. Huber, S. Tanguy, J.-C. Béra, and B. Gilles. A time splitting projection scheme for compressible two-phase flows. application to the interaction of bubbles with ultrasound waves. *J. Comput. Phys.* , 302:439–468, 2015.

[18] Grégory Huber, Sébastien Tanguy, Michael Sagan, and Catherine Colin. Direct numerical simulation of nucleate pool boiling at large microscopic contact angle and moderate jakob number. *International Journal of Heat and Mass Transfer*, 113:662–682, 2017.

[19] M. Ishii and T. Hibiki. *Thermo-Fluid dynamics of two-phase flow*. Springer-Verlag New York, 2 edition, 2011.

[20] M. Jemison, M. Sussman, and M. Arienti. Compressible, multiphase semi-implicit method with moment of fluid interface representation. *J. Comput. Phys.* , 279:182–217, 2014.

[21] W. Kays, M. Crawford, and B. Weigand. *Convective heat and mass transfer*. Mc. Graw Hill, 4 edition, 2003.

[22] M. B. Kuhn and O. Desjardins. An all-mach, low-dissipation strategy for simulating multiphase flows. *J. Comput. Phys.* , 445:110602, 2021.

[23] N. Kwatra, J. Su, J. T. Grétarsson, and R. Fedkiw. A method for avoiding the acoustic time step restriction in compressible flow. *J. Comput. Phys.* , 228:4146–4161, 2009.

[24] Benjamin Lalanne, Lucia Rueda Villegas, Sébastien Tanguy, and Frédéric Risso. On the computation of viscous terms for incompressible two-phase flows with level set/ghost fluid method. *J. Comput. Phys.* , 301:289–307, 2015.

[25] J. Lekner. Parametric solution of the van der waals liquid-vapor coexistence curve. *Am. J. Phys.*, 50(2):161, 1982.

[26] Z. Liu, Y. Lia, G. Lei, Siqi Xia, and Cui Li. Experimental study on refrigeration performance and fluid thermal stratification of thermodynamic vent experimental study on refrigeration performance and fluid thermal stratification of thermodynamic vent. *Int. J. Refrig.* , 88:496–505, 2018.

[27] L. Germez Martinez, B. Duret, J. Reveillon, and F. X. Demoulin. A new dns formalism dedicated to turbulent two-phase flows with phase change. *Int. J. Multiphase Flow* , 143:103762, 2021.

[28] M.Bibal, M. Deferrez, S. Tanguy, and A. Urbano. A compressible solver for two phase-flows with liquid-vapour phase change. applications to bubble cavitation. *J. Comput. Phys.* , 2023. submitted.

[29] T. Ménard, S. Tanguy, and A. Berlemont. Coupling level set/vof/ghost fluid methods: validation and application to 3d simulation of the primary break-up of a liquid jet. *Int. J. Modern Physics C* , 33:510–524, 2007.

[30] S. Mirjalili, S. S. Jain, and M. S. Dodd. Interface-capturing methods for two-phase flows. an overview and recent developments. In *Annual Research Briefs*. CTR, 2017.

[31] NASA. Nasa technology roadmaps ta 14: Thermal management systems, 2015.

[32] Yen Ting Ng, Chohong Min, and Frederic Gibou. On two-phase flow solvers in irregular domains with contact line. *J. Comput. Phys.* , 321:8807–8829, 2009.

[33] W. U. Notardonato, A. M. Swanger, J. E. Fesmire, K. M. Jumper, W. L. Johnson, and T M Tomsik. Zero boil-off methods for large-scale liquid hydrogen tanks using integrated refrigeration and storage. *IOP Conf. Series: Materials Science and Engineerin1g23*, 278:012012, 2017.

[34] K.J. Petersen, S. Rahbarimanesh, and J.R. Brinkerhoff. Progress in physical modelling and numerical simulation of phase transitions in cryogenic pool boiling and cavitation. *Applied Math Modeling* , 116:327–349, 2023.

[35] M.G. Rodio, M.G. De Giorgi, and A. Ficarella. Influence of convective heat transfer modeling on the estimation of thermal effects in cryogenic cavitating flows. *Int. J. Heat and Mass Transfer* , 55:6538–6554, 2012.

[36] Lucia Rueda Villegas, Romain Alis, Mathieu Lepilliez, and Sébastien Tanguy. A ghost fluid/level set method for boiling flows and liquid evaporation: Application to the leidenfrost effect. *Journal of Computational Physics*, 316:789–813, 2016.

DOI: 10.13009/EUCASS2023-329

[37] Ruben Scardovelli and Stéphane Zaleski. Direct numerical simulation of free-surface and interfacial flow. *Ann. Rev. Fluid Mech.* , 31(1):567–603, 1999.

[38] M. Sussman, K. M. Smith, M. Y. Hussaini, M. Ohta, and R. Zhi-Wei. A sharp interface method for incompressible two-phase flows. *J. Comput. Phys.* , 221(2):469–505, 2007.

[39] S. Tanguy and A. Berlemont. Application of a level set method for simulation of droplet collisions. *Int. J. Multiphase Flow* , 31:1015–1035, 2005.

[40] S. Tanguy, T. Ménard, and A. Berlemont. A level set method for vaporizing two-phase flows. *J. Comput. Phys.* , 221:837–853, 2007.

[41] S. Tanguy, M. Sagan, B. Lalanne, F. Couderc, and C. Colin. Benchmarks and numerical methods for the simulation of boiling flows. *J. Comput. Phys.* , 264:1–22, 2014.

[42] Sébastien Tanguy, Michaël Sagan, Benjamin Lalanne, Frédéric Couderc, and Catherine Colin. Benchmarks and numerical methods for the simulation of boiling flows. *Journal of Computational Physics*, 264:1–22, 2014. Publisher: Elsevier.

[43] A Urbano, M Bibal, and S Tanguy. A semi implicit compressible solver for two-phase flows of real fluids. *J. Comput. Phys.* , 456:111034, 2022.

[44] A. Urbano, S. Tanguy, and C. Colin. Direct numerical simulation of nucleate boiling in zero gravity conditions. *Int. J. Heat and Mass Transfer* , 143:118521, 2019.

[45] A. Urbano, S. Tanguy, G. Huber, and C. Colin. Direct numerical simulation of nucleate boiling in micro-layer regime. *Int. J. Heat and Mass Transfer* , 123:1128–1137, 2018.

[46] Jose O. Valderrama. A generalized patel-teja equation of state for polar and nonpolar fluids and their mixtures. *J. Chem. Eng. Japan* , 23(1):87–91, 1990.

[47] G. Vaudor, T. Ménard, W. Aniszewski, M. Doring, and A. Berlemont. A consistent mass and momentum flux computation method for two phase flows. application to atomization process. *Combust. Flame* , 152:204–216, 2017.

[48] F. Xiao, R. Akoh, and S. Ii. Unified formulation for compressible and incompressible flows by using multi-integrated moments ii: Multi-dimensional version for compressible and incompressible flows. *J. Comput. Phys.* , 213:31–56, 2006.